scientific reports

Check for updates

OPEN

Nanobodies targeting ABCC3 for immunotargeted applications in glioblastoma

Eduardo Ruiz-López[1], Ivana Jovčevska[2], Ruth González-Gómez[1], Héctor Tejero[3], Fátima Al-Shahrour[3], Serge Muyldermans[4] & Alberto J. Schuhmacher[1,5]✉

The cancer "omics" reveal many clinically relevant alterations that are transforming the molecular characterization of glioblastomas. However, many of these findings are not yet translated into clinical practice due, in part, to the lack of non-invasive biomarkers and the limitations imposed by the blood–brain barrier. Nanobodies, camelid single-domain antibody fragments, emerge as a promising tool for immunotargeted applications for diagnosing and treating glioblastomas. Performing agnostic bioinformatic analysis from glioblastoma patient datasets, we identified ATP Binding Cassette subfamily C member 3 (ABCC3) as a suitable target for immunotargeted applications. The expression of *ABCC3* is associated with poor survival and impaired response to temozolomide. Importantly, high expression of *ABCC3* is restricted to glioblastoma, with negligible levels in healthy brain tissue, and further correlates with tumor grade and stemness markers. We identified three immunogenic epitopes of ABCC3 which were used to isolate nanobodies from a glioblastoma-specific phage-display nanobody library. Two nanobodies targeting ABCC3 (NbA42 and NbA213) were further characterized and demonstrated in vivo selective recognition of ABCC3 in glioblastoma xenograft mouse models upon systemic administration. We designate NbA42 and NbA213 as new candidates to implement immunotargeted applications guiding a more personalized and precise diagnosis, monitoring, and treatment of glioblastoma patients.

Glioblastoma is a highly aggressive and heterogeneous primary brain tumor. According to the WHO central nervous system (CNS) 5 classification, glioblastoma is an *Isocitrate Dehydrogenase* (*NADP*(+)) (IDH)-wildtype diffuse and astrocytic grade 4 glioma in adults which presents microvascular proliferation or necrosis or mutation of *Telomerase Reverse Transcriptase* (*TERT*) promoter or amplification of *Epidermal Growth Factor Receptor* (*EGFR*) gene or changes in + 7/ − 10 chromosome copy number[1]. Advances in molecular biology and "omic" sciences (e.g., transcriptomics, genomics, metagenomics, epigenomics, proteomics, metabolomics) provide clinically relevant biomarkers for the further development of powerful tools to study the biology of glioblastoma and to identify novel therapies[2].

Despite advances in the molecular classification of glioblastoma, there is an urgent need to designate novel molecular targets to improve patient management strategies. Overall survival has not changed in past decades and remains at 14.6 months for patients with primary glioblastoma. This life expectancy is reduced to 6.7 months after relapse[3,4]. The current standard of care of glioblastoma patients includes maximal surgical resection, followed by radiotherapy with concomitantly and adjuvant chemotherapy with the alkylating agent temozolomide (TMZ)[3,4]. TMZ is an alkylating prodrug that delivers a methyl group to purine bases of DNA generates O^6-methylguanine in DNA, a cytotoxic lesion removed by O^6-methylguanine DNA methyltransferase (MGMT). Methylation of the *MGMT* promoter results in gene silencing and correlates with better outcome in TMZ-treated glioblastoma patients[5]. Although a tissue sample from surgery or biopsies is often required, genetic alterations and epigenetic modifications have uncovered their relevance towards more personalized treatment strategies. The combination of *IDH1* mutations and *MGMT* promoter methylation status offers a higher predictive potential of survival in glioblastoma patients than either alone[6].

[1]Molecular Oncology Group, Instituto de Investigación Sanitaria Aragón (IIS Aragón), 50009 Zaragoza, Spain. [2]Center for Functional Genomics and Biochips, Institute of Biochemistry and Molecular Genetics, Faculty of Medicine, University of Ljubljana, Ljubljana, Slovenia. [3]Bioinformatics Unit, Centro Nacional de Investigaciones Oncológicas (CNIO), 28029 Madrid, Spain. [4]Cellular and Molecular Immunology, Vrije Universiteit Brussel, Pleinlaan 2, 1050 Brussels, Belgium. [5]Fundación Aragonesa para la Investigación y el Desarrollo (ARAID), 50018 Zaragoza, Spain. ✉email: ajimenez@iisaragon.es

A hurdle in diagnosing, monitoring, and treating glioblastoma is imposed by the blood–brain barrier (BBB) by limiting the effectiveness of most of the strategies against this tumor. This highly selective filter restricts access from the bloodstream into the brain parenchyma for almost 100% for large molecules and more than 98% for all small-molecule drugs targeting the CNS[7]. Molecules showing both lipophilic solubility (formation of less than eight hydrogen bonds with solvent water) and MW < 400 Da may be transported through the BBB via lipid-mediated free diffusion[8]. Although drug reengineering contributes to BBB transcytosis, pharmacologically significant amounts of many CNS targeting drugs are unreachable, leading to treatment failure. The range of access of proteins in the blood to the CNS is only 0.01–0.4%, including antibodies with intrinsic therapeutic potential[9]. A wide variety of smaller protein scaffold-based drugs is being developed to circumvent BBB selectivity[10].

Nanobodies represent an innovative alternative due to their reduced size (12–15 kDa; 2.5 nm × 4 nm), constituting one of the smallest molecules with intact functional antigen-recognition capacity[11]. Nanobodies are single-domain antigen-recognizing fragments from the heavy-chain-only antibodies of *Camelidae*. They contain three Complementarity Determining Regions (CDRs) with, on average, larger hypervariable H1 and H3 antigen-binding loops than human antibodies[12]. These characteristics enable nanobodies to recognize unique conformational epitopes, such as cavities or unstructured regions of proteins, with high affinity and stability[13,14]. Besides, various molecular mechanisms for delivering nanobodies through the BBB have been extensively described. Nanobodies targeting CNS molecules have been characterized to cross the BBB by receptor-mediated transcytosis and adsorptive-mediated transcytosis. In this regard, nanobodies have also been utilized not only as shuttle platforms for modeling BBB-permeable drugs but they also have served to improve the targeting of multifunctional therapies (e.g., based on nanoparticles) into the brain parenchyma[15,16].

Performing agnostic bioinformatic analysis in multiple datasets of glioblastoma patients, we identified differentially expressed genes coding for proteins located in the plasma membrane. Among them, we selected ATP-Binding Cassette subfamily C member 3 (ABCC3, also known as MRP3) as a biomarker of glioblastoma, suitable for further development of immunotargeted applications with clinical impact. The ABC transporter superfamily comprises the largest family of proteins for translocating substrates across membranes[17]. Nine of the ABCC subfamily members are designated multidrug resistance proteins (MRPs), as they mediate cancer multidrug resistance (MDR) by actively extruding chemotherapeutic agents out from tumor cells, constituting targets for cancer therapy[18]. Among them, ABCC3 is an organic anion transporter responsible for effluxing anticancer compounds[19,20]. ABCC3 has been involved in chemotherapy failure and reduced survival in various cancers[21,22]. Also, several reports have elucidated a plausible role of ABCC3 in the pathology and prognosis of glioblastoma patients[23,24]. ABCC3 may constitute a promising target for future molecularly targeted clinical intervention of glioblastoma.

We have isolated several nanobodies targeting ABCC3 by following a peptide-based strategy for biopanning of a previously constructed glioblastoma-specific phage-displayed library[25]. Five of these nanobodies showed in vitro specific binding of ABCC3 transporter expressed on the cell surface. Two nanobodies, NbA42 and NbA213, were further characterized and demonstrated selective recognition of ABCC3 transporter in vivo upon systemic administration in glioblastoma xenograft mouse models. Therefore, we propose that NbA42 and NbA213 could serve as molecular candidates for developing immunotargeted applications that could improve the diagnosis, monitoring and therapy of glioblastoma patients.

Results

ABCC3 is a target for glioblastoma immunotargeted applications. Candidate targets of glioblastoma for the development of immunotargeted applications were selected based on (1) their higher gene expression on glioblastoma compared with healthy tissue, and (2) the location of the encoded protein on the extracellular surface of the plasma membrane. To identify the most differentially expressed genes in glioblastoma, we performed a bioinformatic analysis of 142 glioblastoma and 5 normal brain samples (RNA-Seq) deposited in The Cancer Genome Atlas (TCGA)[26] using *limma* (v. 3.24.15, R package)[27]. According to these criteria, 287 genes (Supplementary Table S1) were identified and ranked by differential expression (Log_2FC). 9 genes were identified to be the most differentially expressed in glioblastoma compared to healthy tissue ($Log_2FC > 4$) encoding for membrane-associated proteins (Fig. 1a). Further analysis using GlioVis[28] revealed that only the expression of *ABCC3* and *CA9* correlated with worse patient overall survival (Fig. 1b, and Supplementary Figs. S1a, S1d, S2). The role of CA9 in glioblastoma has been described[29] and nanobodies against CA9 have been previously developed[30]. In addition, the implication of ABCC3 in drug resistance and stemness potential of a variety of tumors has been described[20]. Therefore, we further investigated the role of ABCC3 in glioblastoma.

Despite studies that have suggested higher *ABCC3* expression levels in *MGMT* methylated patient samples[20], we found similar *ABCC3* levels of expression independently of the *MGMT* methylation status (Fig. 1c). Importantly, we found that higher expression of *ABCC3* in patients with methylated *MGMT* promoter correlates with a worse prognosis (Fig. 1d). A possible role for ABCC3 in TMZ resistance and cancer stemness could be hypothesized in glioblastoma. Importantly, we found a correlation between the expression of stemness markers (*CD44* and *FUT4* (*CD15*)) with *ABCC3* in glioblastoma (Fig. 1e, and Supplementary Fig. S1c,d,h,i). *ABCC3* presents lower expression levels in normal brain than in glioblastoma samples (Fig. 1f, and Supplementary Fig. S3), and its expression increases with glioma tumor grade (Figs. 1g, and Supplementary Fig. S1b,e). *ABCC3* is located on human chromosome 17 and its expression in glioblastoma is independent of copy number alterations (Fig. 1h) suggesting that *ABCC3* expression is a regulated process during glioblastoma development instead of a consequence of chromosomal instability (e.g., duplication, deletion, or *loci* amplification). We also observe high levels of expression of ABCC3 in a panel of glioblastoma cell lines (Fig. 1i). These data point to ABCC3 as a suitable molecular target that meets the requirements for further developing nanobody-based immunotargeted tools for glioblastoma.

a

RANK	GENE	Log_2FC	*P* value
1	UBE2C	8,29	1,6701E-13
2	ABCC3	5,30	0,00303263
3	GTSE1	5,29	4,131E-08
4	CA9	5,17	0,00717801
5	ASPM	4,93	2,4757E-06
6	IQGAP2	4,78	2,5543E-07
7	CKAP2L	4,33	1,2522E-07
8	SKA3	4,20	1,2481E-06
9	KIF18B	4,06	0,00012271

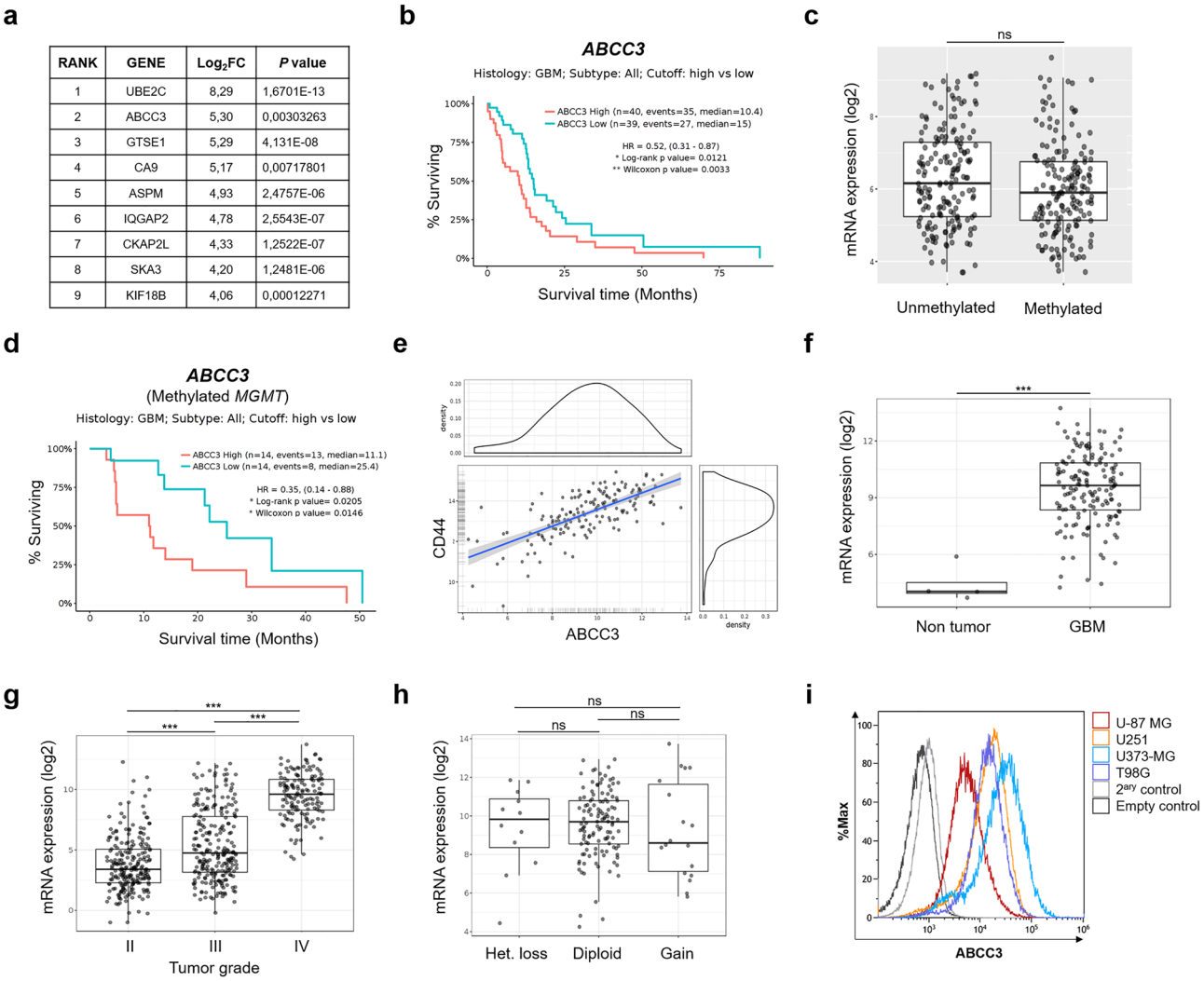

Figure 1. ABCC3 is highly expressed in glioblastoma and correlates with poor prognosis. (**a**) List of membrane-associated genes differentially expressed in glioblastoma vs. normal tissue ($Log_2FC > 4$; data from TCGA, https://www.cancer.gov/tcga[26], accessed on April 26th, 2017): *Ubiquitin Conjugating Enzyme E2 C* (*UBE2C*), *ATP Binding Cassette subfamily C member 3* (*ABCC3*), *G2 And S-Phase Expressed 1* (*GTSE1*), *carbonic anhydrase 9* (*CA9*), *Assembly Factor For Spindle Microtubules* (*ASPM*), *IQ Motif Containing GTPase Activating Protein 2* (*IQGAP2*), *Cytoskeleton Associated Protein 2 Like* (*CKAP2L*), *Spindle And Kinetochore Associated Complex Subunit 3* (*SKA3*), and *Kinesin Family Member 18B* (*KIF18B*). (**b**) Kaplan–Meier curves for overall survival in the TCGA-GBM dataset (RNA-Seq, GlioVis) for ABCC3. (**c**) *ABCC3* expression is independent of *MGMT* methylation status. Tukey's Honest Significant Difference (HSD). TCGA-GBM dataset (RNA-Seq, GlioVis). The figure shows the difference between pairs (mean ± SEM), the 95% confidence interval and the p-value of the pairwise comparisons; ns, non significant. (**d**) Kaplan–Meier curves for overall survival in the TCGA-GBM dataset (RNA-Seq, GlioVis) for *ABCC3* in *MGMT* methylated patients. Log-rank and Wilcoxon test for survival curves. Cut off top high vs low. $^{**}p < 0.01$; $^{*}p < 0.05$. (**e**) Correlation of *ABCC3* and *CD44* expression. Pearson's product-moment correlation. TCGA-GBM dataset (RNAseq, GlioVis). $^{***}p < 0.001$. (**f**) *ABCC3* expression in glioblastoma (n = 156) and control brain (n = 4) (ATCC-GBM dataset, RNA-Seq, GlioVis; mean ± SEM). (**g**) *ABCC3* expression increases with tumor grade (ATCC-GBMLGG dataset, RNA-Seq GlioVis; mean ± SEM). Grade II (n = 226), Grade III (n = 224), Grade IV (n = 150). (**h**) *ABCC3* expression and copy number alterations (CNA) from the ATCC-GBM dataset (RNA-Seq, GlioVis; mean ± SEM). Heterozygous loss (n = 12), Diploid (n = 121), Gain (n = 18). HSD test for (f), (g) and (h). $^{***}p < 0.001$; $^{**}p < 0.01$; $^{*}p < 0.05$; ns, (**i**) ABCC3 expression in U-87 MG, U251, U373-MG, and T98G glioblastoma cell lines determined by flow cytometry. Empty control consists of unstained cells.

Selection of three immunogenic epitopes of ABCC3 as suitable targets. A glioblastoma-specific phage-display library of nanobodies with ~ 1×10^8 transformants was previously constructed[25]. Screening and selection of nanobodies targeting ABCC3 were performed following a peptide-based strategy. We predicted immunogenic epitopes within the amino acidic sequence of ABCC3 (UniProtKB reference: O15438) using BepiPred-2.0 analy-

a

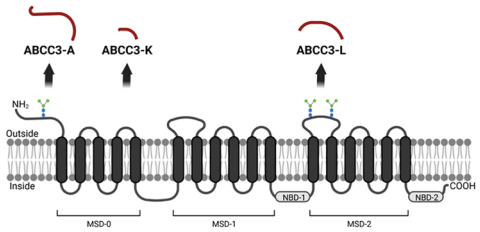

ABCC3-derived peptide	Aminoacid sequence	Aminoacid position	ABCC3 domain
ABCC3-A	ALCGSGELGSKFWDSNLSVHTENPDLTPCF	3-32	N-terminus
ABCC3-K	KAEGEISDPFR	160-170	2nd extracellular loop
ABCC3-L	SAWTNDAMADSRQNNTSL	993-1010	6th extracellular loop

b

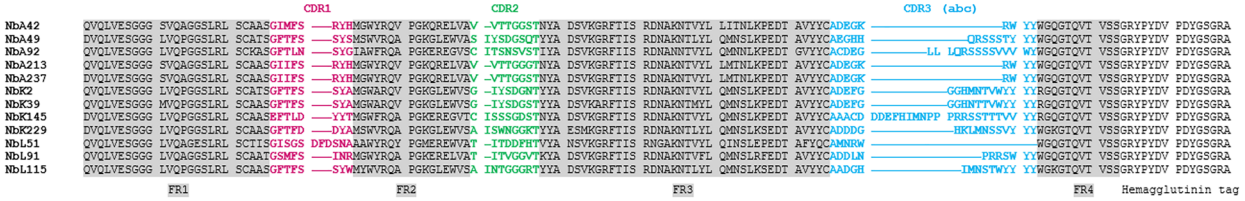

c

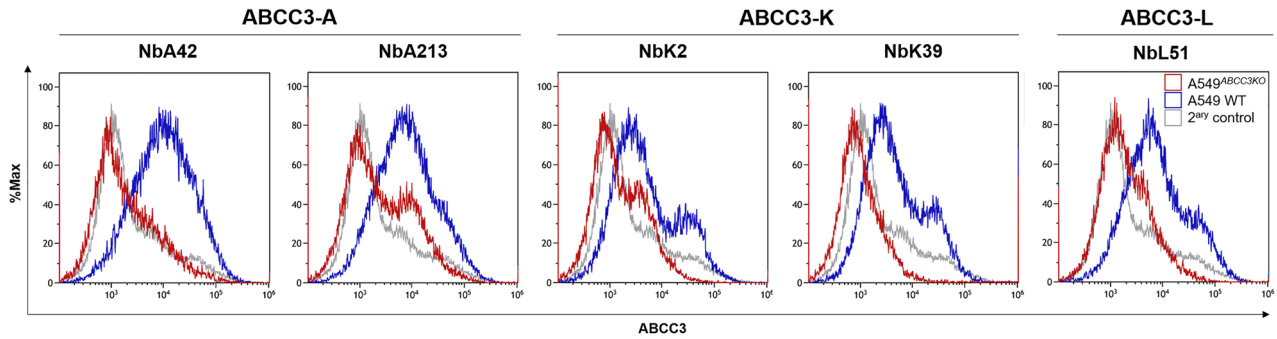

Figure 2. Identification of nanobodies targeting ABCC3 following a peptide-based strategy for biopanning. (**a**) Proposed membrane topology of ABCC3 (UniProtKB reference: O15438). ABCC3 comprises two Membrane Spanning Domains (MSD-1 and MSD-2), each of them containing 6 transmembrane helices and followed by one Nucleotide-Binding Domain (NBD-1 and NBD-2), and an additional N-terminal domain containing 5 transmembrane helices (MSD-0). Extracellular N-glycosylation sites may regulate substrate specificity, stability, and localization of ABCC3[19]. The location and amino acid sequence of the selected peptides in extracellular regions utilized to isolate specific nanobodies targeting ABCC3 from a phage display library is shown. (**b**) Amino acid sequence of the isolated nanobodies targeting ABCC3 depicting their Framework Regions (FR1-4, grey) and Complementarity Determining Regions (CDR1, pink; CDR2, green; and CDR3, given in alphabetic order, blue). Nanobodies NbA49, NbK2, NbK39, NbK229 and NbL115 present a VH-like VHH imprint in their framework 2 region (GLEW sequence). Nanobody NbL51 presents an extremely short CDR3 domain, which the longer CDR1 loop might compensate for, and a modified GLEW motif with a three-amino acid insertion. Some nanobodies targeting ABCC3 have an R118 residue instead of W118 as the first amino acid of the framework 4 region, which is exclusive of VHHs and not presented in humans, mouse nor camel VH. (**c**) Screening of the immunoreactivity of nanobodies targeting ABCC3 by flow cytometry. The immunoreactivity of 2 nanobodies targeting peptide ABCC3-A (NbA42, NbA213), 2 nanobodies targeting peptide ABCC3-K (NbK2, NbK39), and 1 nanobody targeting peptide ABCC3-L (NbL51) was confirmed. A549 cell line (A549 WT) and its ABCC3 knocked-out derivative cell line (A549^{ABCC3KO}) were used as positive and negative controls. Secondary staining controls are also shown.

sis software[31]. Candidate immunogenic epitopes were selected based on (1) their sequential nature, as linear B-cell epitopes are commonly used for immunizations and antibody production[32], (2) their length, with limitation to a minimum of 11 and a maximum of 30 amino acids to approximate the size of current linear epitopes[33,34], and (3) their outer surface location at the plasma membrane, restricted to extracellular regions of the Membrane Spanning Domains (MSDs) and N-terminus of ABCC3 (Fig. 2a). The bioinformatic analysis yielded 57 potential immunogenic epitopes (Supplementary Table S2), from which four peptides met these requirements. Their precise alignment with the ABCC3 sequence was confirmed utilizing the Basic Local Alignment Search Tool (BLAST) Protein (BlastP). As shown in Fig. 2a, one of the selected peptides (ABCC3-A, amino acids 3–32) is located in the N-terminus, while the other three (ABCC3-K, amino acids 160–170; ABCC3-V, amino acids 557–569; and ABCC3-L, amino acids 993–1010) are located within extracellular loops of MSDs of ABCC3. Three of them were synthesized with an addition of a 6× His-tag at the C-terminus (ABCC3-A and ABCC3-K) or N-terminus (ABCC3-L), for further screening of nanobodies.

Identification and screening of nanobodies targeting ABCC3. For nanobody enrichment, each ABCC3-derived peptide was used for three rounds of biopanning of the phage-display library[25]. We identified 12 nanobodies with different and complete sequences (Fig. 2b; Supplementary Table S3). We selected five nanobodies recognizing peptide ABCC3-A (NbA42, NbA49, NbA92, NbA213, NbA237), four nanobodies with ABCC3-K (NbK2, NbK39, NbK145, NbK229), and three nanobodies with ABCC3-L (NbL51, NbL91, NbL115). The selective targeting of the isolated nanobodies against ABCC3 was evaluated by flow cytometry (Supplementary Figure S4a). The human lung adenocarcinoma A549 cell line (A549 WT) presents the highest levels of ABCC3 expression (Human Protein Atlas, http://www.proteinatlas.org)[35] and was selected as a positive control for the initial experiments. We knocked-out ABCC3 by CRISPR/Cas9 technology. The resulting cell line ($A549^{ABCC3KO}$) was used as a negative control (Supplementary Fig. S4b).

Five nanobodies showed significant differential binding capacity (Fig. 2c). The immunoreactivity of two nanobodies targeting peptide ABCC3-A (NbA42, NbA213), two nanobodies targeting peptide ABCC3-K (NbK2, NbK39), and one nanobody targeting peptide ABCC3-L (NbL51) was confirmed. NbA42 and NbA213 were the nanobodies with the highest potential to detect ABCC3 in vitro and were further evaluated.

Molecular characterization of anti-ABCC3 nanobodies. *Nanobodies NbA42 and NbA213 specifically recognize ABCC3.* The potential of targeting ABCC3 by NbA42 and NbA213 was evaluated by flow cytometry using ABCC3-expressing and loss-of-function control cell lines (Fig. 3a), demonstrating the potential to discriminate different proportions of these cell types in vitro. Subsequently, both nanobodies were labeled with fluorescein-5-isothiocyanate (FITC) to determine their equilibrium dissociation constant (K_D). The affinity of NbA42 and NbA213 was assessed by targeting the control cell line A549 WT, using $A549^{ABCC3KO}$ as a non-specific background control (Fig. 3b). Results showed that both nanobodies bind whole-length ABCC3 protein in vitro ($K_D = 115.3 \pm 89.95$ μM for NbA42 and $K_D = 52.58 \pm 25.79$ μM for NbA213). We confirmed the specific recognition of NbA42 and NbA213 to peptide ABCC3-A among the other ABCC3-derived peptides (e.g., ABCC3-K, and ABCC3-L) by indirect ELISA (Fig. 3c). The combination of NbA42 and NbA213 demonstrated no synergy to detect ABCC3 in vitro (Fig. 3d), further validating the common recognition of peptide ABCC3-A.

NbA42 and NbA213 can target ABCC3 in vivo. The capacity of NbA42 and NbA213 to target ABCC3 in vivo was evaluated in xenografted tumor-bearing mice of the A549 and $A549^{ABCC3KO}$ control cell lines. Nanobodies were administered intraperitoneally (i.p.) at 15 $mg{\cdot}kg^{-1}$ and their specific binding was analyzed 1 h after systemic injection (Fig. 4a). Similar to the in vitro data, systemic injection of NbA42 and NbA213 demonstrated selective detection of ABCC3 in vivo (Fig. 4b). Both nanobodies specifically bound A549 WT xenografted tumors (ABCC3-expressing cells), compared with the background of $A549^{ABCC3KO}$ xenografted tumors (ABCC3-loss-of-function cells). NbA42 and NbA213 showed minimal residual signals in other tissues (Supplementary Fig. S5a). Accordingly to previously reported data on the pharmacokinetic profile of other nanobodies[36–38] NbA42 and NbA213 were early detected in blood plasma after i.p. administration and cleared from circulation by renal clearance (Supplementary Fig. S5b). NbA42 and NbA213 were not detectable in plasma samples 4 h upon systemic administration.

NbA42 and NbA213 also target ABCC3-expressing glioblastoma cell lines. Both nanobodies showed a similar in vitro targeting of ABCC3 in U-87 MG, U251 and T98G cells (Supplementary Fig. S6). We next evaluated the capacity of NbA42 and NbA213 to selectively target glioblastoma cells in vivo. First, we analyzed the selective targeting of NbA42 and NbA213 in U-87 MG and T98G heterotopic xenografted tumor-bearing mice in vivo (Fig. 4c). One hour after systemic administration, both nanobodies recognized ABCC3-expressing heterotopic xenografted glioblastoma tumors. We next evaluated the potential of NbA42 and NbA213 to detect ABCC3-expressing orthotopic brain tumors (Fig. 5a). Two orthotopic glioblastoma mouse models, with different degrees of BBB disruption, were utilized. As expected, U-87 MG derived tumors presented a higher degree of damaged integrity of the BBB than U251 derived tumors (Fig. 5b). Both, NbA42 and NbA213, detected either both U-87 MG and U251 orthotopic brain tumors (Fig. 5c) suggesting that these nanobodies does not present a high dependence for a highly disrupted BBB. Altogether, these results point to NbA42 and NbA213 as candidates for further development of immunotargeted applications for glioblastoma diagnosis and/or therapy.

Discussion

"Omic" sciences hold the promise of precision medicine in cancer by translating molecular-based big data into novel clinical approaches[39]. Performing agnostic bioinformatic analysis across multiple datasets we identified ABCC3 as a suitable candidate to develop immunotargeted tools for glioblastoma. ABCC3 transporter is a member of the multidrug resistance proteins (MRPs) which confers resistance to various chemotherapeutic anticancer compounds[19]. In agreement with other reports we found that *ABCC3* is highly expressed in glioblastoma samples, correlates with tumor grade and worse prognosis of patients[23,24].

ABCC3 may have a plausible role in temozolomide (TMZ) resistance. The expression of ABCC3 increases following TMZ treatment in glioblastoma cell lines, in a concentration and time-dependent manner[40,41]. Also, the specific inhibition of ABCC3 with MK571 increases apoptosis upon TMZ treatment in other cell types[42]. The higher expression of ABCC3 in NK cells modulates their chemoresistance to TMZ in patients of malignant gliomas[43]. Recently, *ABCC3* has been included in gene signatures (*ABCC3*, *CD44*, *TNFRSF1A*, and *MGMT*[24]; *ABCC3*, *SMC4*, *EMP3*, *WEE1*, and *HIST1H2BK*[44]) that classify glioma patients in agreement with therapeutic response to chemotherapeutic agents, including TMZ. According to previous reports[20], we found higher *ABCC3* expression in patients with methylated *MGMT* promoter, correlating with a worse prognosis. A role of ABCC3 in cancer stemness is emerging, as *ABCC3* knockdown reduced the expression of stemness genes and the $CD44^{high}/CD24^{low}$ breast cancer stem-like subpopulation. Also, SOX2 mediates transcription of *ABCC3* in

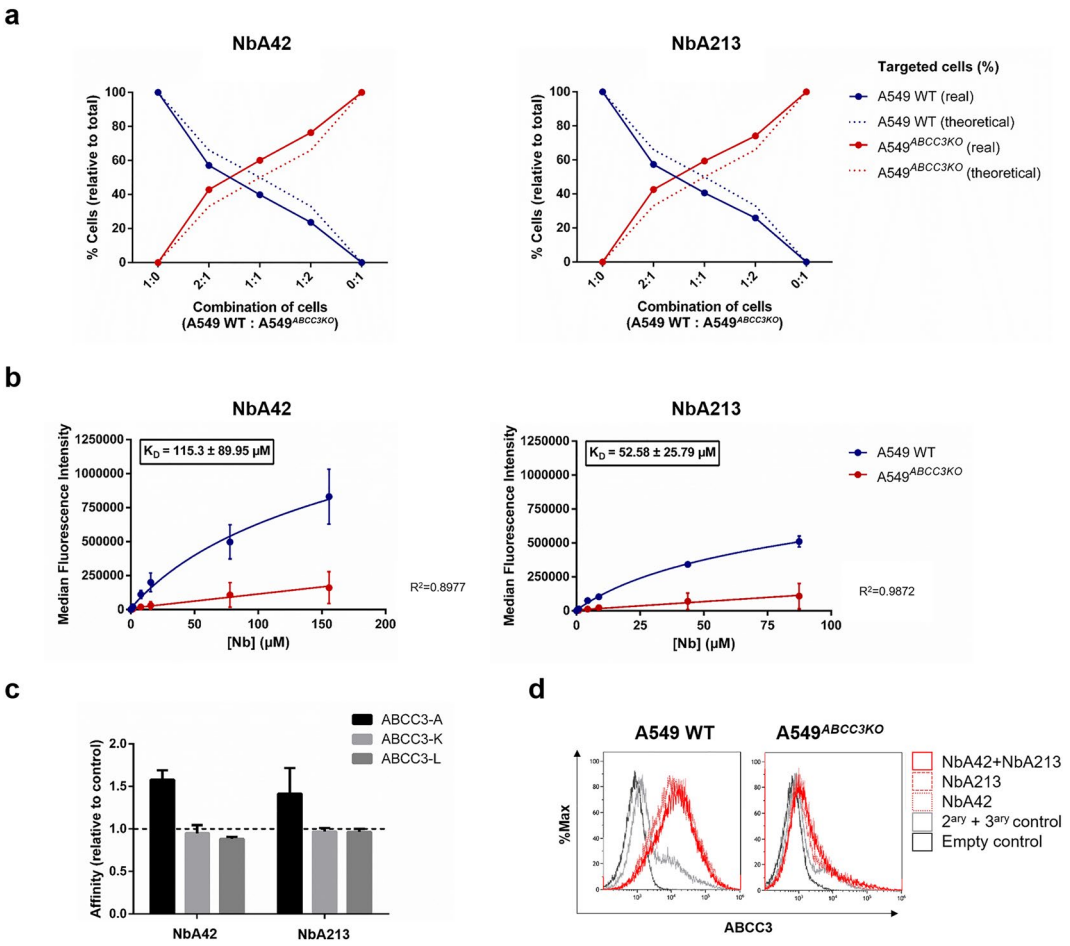

Figure 3. Evaluation of the targeting potential of NbA42 and NbA213 against ABCC3. (**a**) NbA42 and NbA213 specifically target ABCC3-expressing cells (A549 WT) over A549^{ABCC3KO} control cell line by flow cytometry. Both cell lines were combined at different proportions. Percentage of targeted cells, relative to the total number of cells, is shown for each proportion (X axis). Theoretical percentages of targeted cells, given by each ratio, have been included (dotted line). (**b**) Binding affinity of NbA42 and NbA213. Their equilibrium dissociation constant (K_D) was calculated by flow cytometry (n = 2). Increasing concentrations of FITC-labeled nanobodies were used to quantify ABCC3 expression in A549 WT and A549^{ABCC3KO} control cell lines. (**c**) Binding specificity of NbA42 and NbA213. The selective binding to the ABCC3 peptide used for their isolation by biopanning (e.g., ABCC3-A, ABCC3-K and ABCC3-L) was calculated by indirect ELISA. The dark dotted line represents the background signal yielded by the negative control (0.1 M $NaHCO_3$ coating buffer without peptide) (n = 2). (**d**) Dual-nanobody flow cytometry to evaluate synergies in the detection of ABCC3 in vitro.

glioblastoma cells[45]. We found a similar correlation between *CD44*, *FUT4* (*CD15*) and *ABCC3* expression across glioblastoma patient datasets. These data support the possible intervention of ABCC3 in TMZ resistance and cancer stemness. Then, ABCC3 could represent a new molecular target of glioblastoma which may facilitate the subsequent development of molecular imaging approaches for patient management.

Novel immunotargeted applications obtained by combining the selectivity of antibody derivatives with the resolution capabilities of a given imaging modality, have been implemented for glioblastoma theragnosis. Single-chain variable fragments (scFvs) against ABCC3 have been used in preclinical models of glioblastoma. Interestingly, scFvs M25, M58, and M89 recognized extracellular epitopes of the N-terminus of ABCC3 and showed specific targeting of ABCC3-expressing glioblastoma cells in vitro[46]. However, the access of scFvs into the CNS is limited and fusion to cell-penetrating peptides acting as BBB shuttles is often required[47]. Nanobodies can circumvent the BBB by taking advantage of molecular routes of transcytosis[15,16]. In recent years, several nanobodies have sprouted against glioblastoma targets of protein biosynthesis (TUFM, TRIM28), DNA metabolism (NAP1L1), and cellular growth (EGFR, DPYSL2, β-Actin)[48–50]. Here, we describe two novel nanobodies targeting ABCC3, NbA42 and NbA213, isolated from a previously constructed glioblastoma-specific phage-display library[25]. The rational design of immunogenic-like peptides located on the extracellular surface of ABCC3 allowed a peptide-based strategy for biopanning. In vitro studies showed that NbA42 and NbA213 specifically target ABCC3 at the N-terminus (peptide ABCC3-A). NbA42 and NbA213 recognized ABCC3-expressing cells in glioblastoma heterotopic xenografted tumor-bearing mice. Detection of ABCC3 by NbA42 and NbA213 was further achieved in two orthotopic glioblastoma mouse models with different degrees of BBB disruption. While

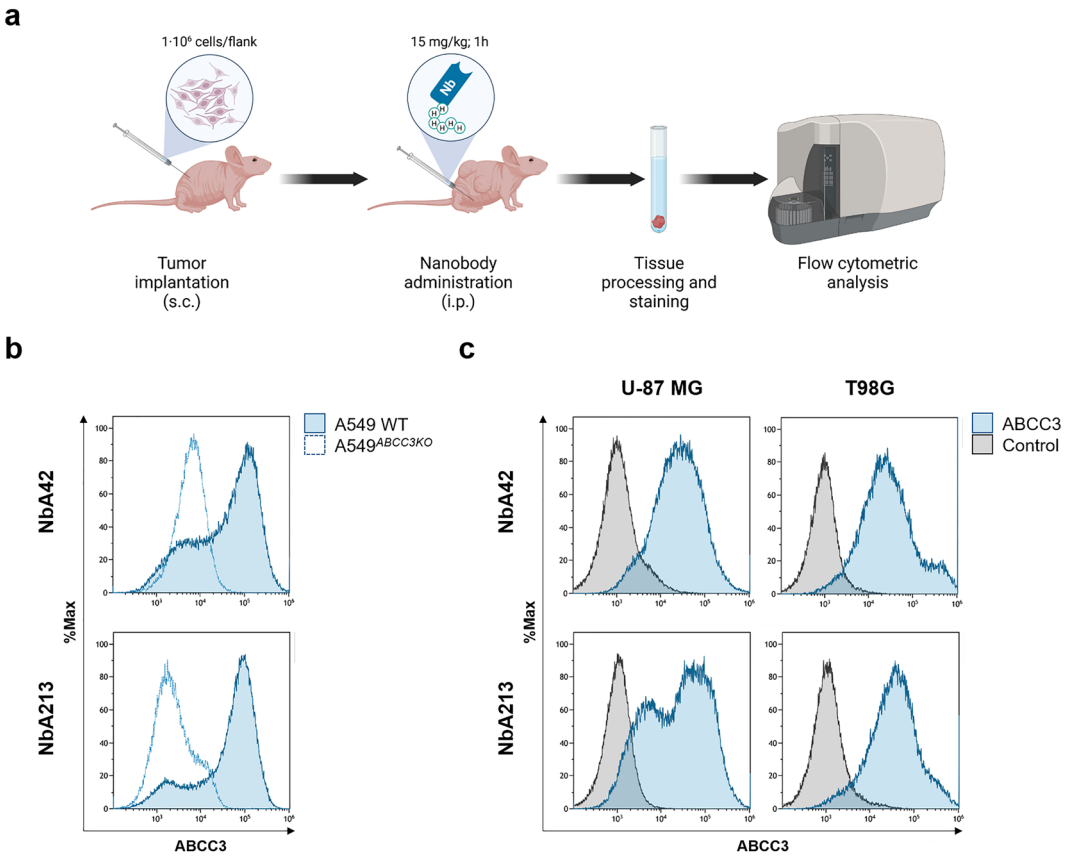

Figure 4. NbA42 and NbA213 recognize ABCC3-expressing tumors in vivo. (**a**) Workflow of the experimental setup of targeting analysis of nanobodies. Nanobodies were administered at 15 mg·kg^{-1} intraperitoneally (i.p.) in xenografted mice with the indicated cell lines, and tumor targeting was examined using prospective ex vivo flow cytometry, 1 h after systemic injection. Image created with BioRender.com (accessed on November 19th, 2021). (**b**) Evaluation of the in vivo targeting of NbA42 and NbA213 in ABCC3-expressing and loss-of-function cell lines (e.g., A549 WT, and A549^{ABCC3KO}). (**c**) Assessment of the potential detection of ABCC3-expressing glioblastoma tumors by NbA42 and NbA213 in vivo.

further characterization of the BBB penetrance is required, these results suggest that these nanobodies do not present a high dependence on a highly disrupted BBB. Future applications of both nanobodies targeting ABCC3 may allow the development of novel glioblastoma theragnostic procedures.

Nanobodies constitute a versatile tool for cancer management[51]. Among others, nanobodies have been exploited to deliver cytotoxic payloads specifically to tumors, image-guided surgery, and to improve chimeric antigen receptor (CAR)-T and photodynamic therapies[52–56]. Since the approval of nanobody ALX-0681 (Caplacizumab) by the regulatory agencies[57], examples of radiolabeled nanobodies conducting immuno-positron emission tomography (immuno-PET)[58] studies have reached clinical trials in cancer patients. Regarding glioblastoma, ^{89}Zr-labeled nanobodies targeting HGF have demonstrated their theragnostic potential in preclinical models[59]. We highlight the potential of NbA42 and NbA213 as new candidate molecules for the further design of nanobody-based molecular imaging probes. The predictive role of ABCC3 in the survival and prognosis of glioblastoma patients reveals a newfangled translational diagnostic and/or therapeutic relevance of NbA42 and NbA213 in the clinics.

Materials and methods

Cell cultures. Human lung adenocarcinoma A549 and its ABCC3 knocked-out by CRISPR/Cas9 system derivative A549^{ABCC3KO} cell lines, and U-87 MG, U251, U373-MG, and T98G human glioma cell lines were grown with DMEM medium (Sigma-Aldrich) containing 10% FBS (Fisher Scientific), and maintained at 37 °C and 5% CO_2. A549 and U373-MG were kindly provided by Dr. Martín-Duque (IACS). U-87 MG, U251, and T98G were kindly provided by the Holland and Joyce laboratories (MSKCC). Short tandem repeat markers performed cell line authentication at different passages.

Bioinformatic analysis and statistics. RNA-Seq data from 142 glioblastoma samples and 5 normal brain samples deposited in The Cancer Genome Atlas (TCGA; https://www.cancer.gov/tcga accessed on April 26th, 2017)[26] were analyzed using *limma* (v.3.24.15, R package)[27] to identify the most highly expressed genes. The differentially expressed list of genes was mined for those that encode proteins located in the plasma mem-

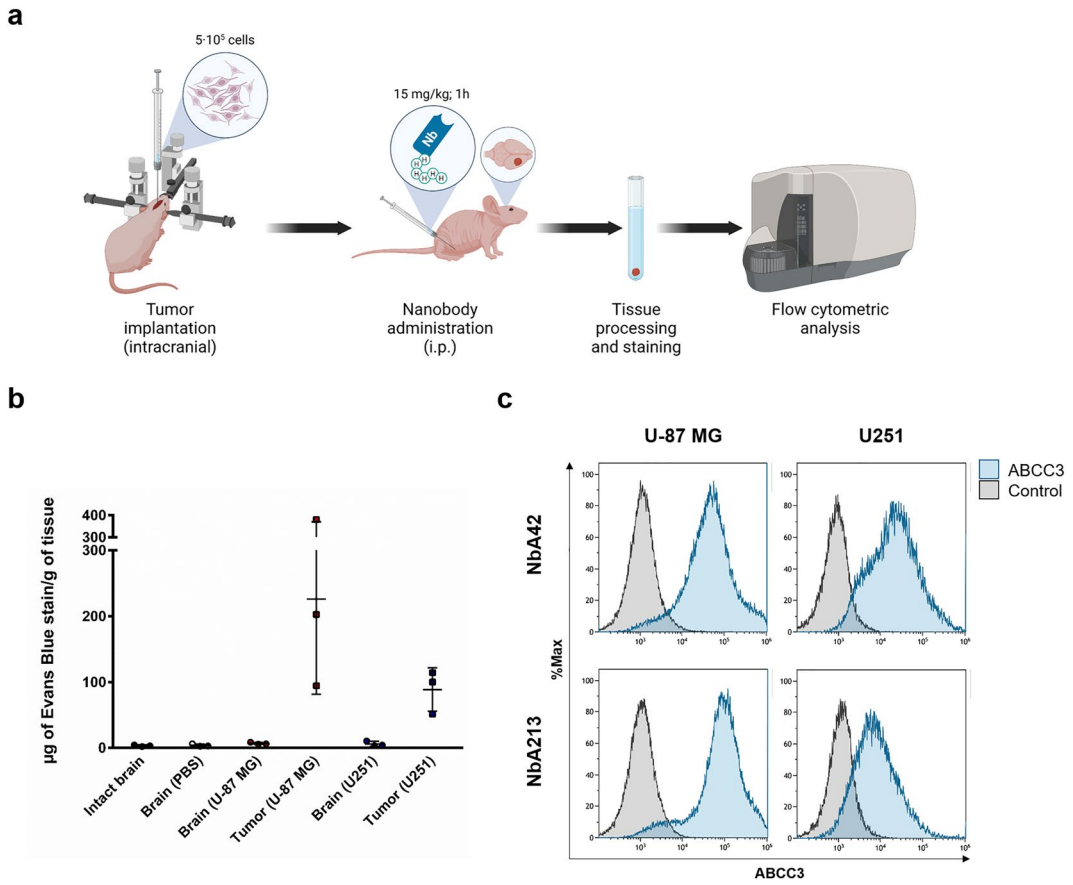

Figure 5. NbA42 and NbA213 recognize ABCC3-expressing orthotopic brain tumors. (**a**) Workflow of the experimental setup of targeting analysis of nanobodies. Nanobodies were administered at 15 mg·kg^{-1} i.p. in mice bearing intracranial glioblastoma tumors generated from the indicated cell lines. Tumor targeting was examined using prospective ex vivo flow cytometry, 1 h after systemic injection. Image created with BioRender.com (accessed on November 5th, 2022). (**b**) Assessment of the potential detection of ABCC3-expressing orthotopically implanted glioblastoma tumors by NbA42 and NbA213. (**c**) Analysis of BBB integrity by quantification of i.p. administered Evans blue in the brain of mice with intact, mock surgery brains (PBS), orthotopic U251 and U-87 MG tumors and their contralateral hemisphere. Graphic depict the amount of Evans blue stain per gram of tissue (mean ± SD; n = 3).

brane. The subcellular localization was determined by experimental immunohistochemistry evidence as cataloged in the Human Protein Atlas (http://www.proteinatlas.org[35], "compartments" database[60]). Gene expression and survival of adult glioblastoma patient data from the TCGA Project (TCGA-GBM and TCGA-GBMLGG), the Chinese Glioma Genome Atlas (CGGA, http://www.cgga.org.cn/ accessed on October 5th, 2021)[61], and the Repository for Molecular Brain Neoplasia Data (REMBRANDT, https://wiki.cancerimagingarchive.net/display/Public/REMBRANDT)[62] were analyzed using GlioVis data portal (http://gliovis.bioinfo.cnio.es/)[28]. Log-rank and Wilcoxon tests were applied for Kaplan–Meier survival curves. Pearson's product-moment correlation was applied to determine gene correlations between paired samples. Tukey's Honest Significant Difference (HSD) was applied to compare *ABCC3* expression across tumor grades and glioblastoma vs. normal samples. Statistical analysis was obtained from GlioVis and completed using R (http://www.r-project.org).

Biopanning of nanobodies. Prediction of immunogenic epitopes of human ABCC3 (UniProtKB reference: O15438) was performed by submitting the amino acidic sequence to BepiPred-2.0 analysis software (IEDB, https://www.iedb.org/ accessed on August 1st, 2018)[31]. A list of 57 potential epitopes was obtained (Supplementary Table S2) and manually curated for those located in the outer part of the plasma membrane. Three peptides, corresponding to immunogenic-like extracellular ABCC3 epitopes, were selected and His-tagged synthesized (Thermo Scientific):

- ABCC3-A (ALCGSGELGSKFWDSNLSVHTENPDLTPCFHHHHHH),
- ABCC3-K (KAEGEISDPFRHHHHHH),
- ABCC3-L (HHHHHHSAWTNDAMADSRQNNTSL).

These peptides were used for biopanning as described elsewhere[63], using an existing phage-display library of nanobodies generated upon immunization of an adult male alpaca with whole patient-derived stem-like-enriched glioblastoma cells[25]. For each ABCC3-derived peptide, the library was subjected to 3 sequential rounds of biopanning by facing 1 µg peptide in 0.1 M $NaHCO_3$, pre-coated on NUNC anti-histidine ELISA plates (Thermo Scientific), with 10^{11} phages for 1 h at room temperature. Non-specific binding sites were blocked with 5% non-fat milk. Bound phages were eluted with 100 mM triethylamine and neutralized with 1 M Tris–HCl (pH 7.4). Phages were used to infect the amber-codon-suppressing TG1 *E. coli* cells for 30 min at 37 °C, which were later co-infected with 10^{15} M13K07 helper phages. Enriched phages were grown overnight at 37 °C in 2× Tryptone & Yeast extract medium supplemented with 100 µg/mL ampicillin and 70 µg/mL kanamycin. New produced phages were precipitated with ice-cold polyethylene glycol-6000/NaCl and resuspended in 1 mL PBS.

Specificity by enzyme-linked immunosorbent assay (ELISA). Nanobodies were expressed in TG1 *E. coli* by adding isopropyl β-D-1-thiogalactopyranoside (IPTG) to cultures at a final concentration of 1 mM and incubating overnight at 28 °C. Extraction of periplasmic proteins including hemagglutinin(HA)-tagged nanobodies was performed by osmotic shock with 4× Tris/EDTA/sucrose and ddH_2O. ELISA was performed by adding bacterial periplasmic extracts to 96-well NUNC MaxiSorp plates (Thermo Scientific), previously coated with 2 µg/mL of ABCC3-derived peptide in 0.1 M $NaHCO_3$ (5 µg/mL for measuring binding specificity). Absorbance at 405 nm was measured on a Synergy HT multi-mode microplate reader (BioTek), after incubation with mouse anti-HA (1:2000; Sigma-Aldrich) and goat anti-mouse IgG conjugated with alkaline phosphatase (1:2000; Sigma-Aldrich) antibodies, and alkaline phosphatase substrate (Sigma-Aldrich). Potential clones targeting ABCC3 rendered 1.5 higher signal than its negative control without antigen. Genetic sequences of specific nanobodies were amplified by colony PCR with primers RP (5'-TCACACAGGAAACAGCTATGAC-3') and GIII (5'-CCACAGACAGCCCTCATAG-3'), and sequenced at Macrogen (The Netherlands).

Production of nanobodies. Nanobodies with complete sequences were recloned from pHEN4[12] into the pHEN6[64] expression vector, to replace their HA-tag by a hexahistidine(His)-tag for further purification. Briefly, similar colony PCR with primers A6E (5'-GATGTGCAGCTGCAGGAGTCTGGAGGAGG-3') and 38 (5'-GGACTAGTG CGGCCGCTGGAGACGGTGACCTGGGT-3') yielded products of 400 bp, further cloned into pHEN6 with *Pst*I and *Bst*EII (*Eco91*I) (Thermo Scientific). Conservation of sequences was verified by PCR with FP (5'-CGCCAGGGTTTTCCCAGTCACGAC-3') and RP (5'-TCACACAGGAAACAGCTATGAC-3'), with further sequencing. Expression of nanobodies encoded in the pHEN6 vector was performed in WK6 *E. coli* as previously described[64]. Briefly, 1 mM of IPTG was added to cultures to induce nanobody expression overnight at 28 ˚C. Periplasmic extracts were obtained by osmotic shock and dialyzed on Spectra/Por dialysis membrane tubing of MWCO 3.5 kDa (Spectrum laboratories, Inc) in PBS. His-tagged nanobodies were purified using an increasing gradient of 0.5 M imidazole on immobilized metal affinity chromatography columns in an ÄKTA protein purification system (GE Healthcare). Nanobody concentration was measured on a Synergy HT multi-mode microplate reader (BioTek) after incubation with Bradford reagent (Bio-Rad Laboratories, Inc).

Flow cytometry. To analyze the expression levels of ABCC3, 4×10^5 cells were counted using a Neubauer chamber using Trypan Blue Solution 0.4% (Fisher Scientific). After incubation in blocking and permeabilizing buffer (PBS/saponin 0.1%/FBS 5%) for 15 min at 4 °C, cells were stained with anti-ABCC3 monoclonal antibody (mAb, 1:150; clone M3II-9; Fisher Scientific) and APC goat anti-mouse IgG antibody (1:1500; clone Poly4053; Biolegend) for 20 min at 4 °C. To stain with nanobodies targeting ABCC3, cells were detached with 10 mM EDTA (Fisher Scientific). Upon incubation in blocking buffer (PBS/1% BSA) for 15 min at 4 °C, cells were stained with 5 µg of anti-ABCC3 nanobody followed by ReadyTag anti-6-His mAb (1:1500; clone 6-HIS, BioXCell) and APC goat anti-mouse IgG antibody (1:1500; clone Poly4053, Biolegend) for 20 min at 4 °C. Cells were analyzed on a Gallios flow cytometer (Beckman Coulter) and results were visualized at Kaluza analysis software (Beckman Coulter). To estimate the equilibrium dissociation constant (K_D), nanobodies were conjugated to fluorescein-5-isothiocyanate using FluoroTag™ FITC Conjugation Kit (Sigma-Aldrich), and total and non-specific binding was analyzed with GraphPad Prism v.6.01.

Animal ethics statement and experimental design. Athymic Nude-Foxn1$^{nu/nu}$ mice were purchased from Envigo (Spain). Mice were housed in animal experimental core facilities of the Aragon Institute of Health Sciences (IACS) at the Biomedical Research Center of Aragon (CIBA, Zaragoza, Spain). All animal experiments were approved and carried out according to the Ethical Committee for Animal Experimentation of the University of Zaragoza, under the protocol project No. PI60/20. Mice were cared for in accordance with the European 2010/63/UE and Spanish national RD1386/2018 legal statements.

Subcutaneous xenograft models were established (1×10^6 cells; 6–8 weeks athymic nude mice). Nanobodies were administered intraperitoneally (i.p.) at 15 $mg{\cdot}kg^{-1}$ in mice bearing tumors (1000 mm^3). Mice were sacrificed 1 h after administration; tumors were mechanically disaggregated and incubated in 10 mM EDTA (Fisher Scientific). The targeting profile of nanobodies was evaluated by prospective ex vivo flow cytometry in collected tissues (liver, kidney, brain, blood, and tumors).

For orthotopic xenografts, U-87 MG and 251 cells were transduced with a TK-GFP-Luciferase reporter plasmid (TGL) to monitor tumor growth by bioluminescence measurements. To develop intracranial tumors, 6–8 weeks athymic nude mice were anesthetized by inhalation of 3% isoflurane and were subcutaneously injected with 50 µL of the local anesthetic 0.25% bupivacaine at the surgical site. Mice were intracranially injected with 2 µL containing $5{\cdot}10^5$ U-87 MG-TGL or 251-MG-TGL cells resuspended in PBS, using a fixed stereotactic apparatus (Stoelting). Injections were made to the right frontal cortex, approximately 1 mm caudal and 1.5 mm lateral

from bregma, and at a depth of 2 mm using a Hamilton syringe (Hamilton) as described previously[65,66]. Tumor growth was monitored by bioluminescence. Mice were injected with D-Luciferin (150 mg/kg). 15 min after injection, images were acquired for 5 s using an IVIS Lumina XRMS equipment (Perkin Elmer). Bioluminescence analysis was performed using Living Image software, version 2.50. Nanobodies were administered as described above in mice with tumors in a positive growth phase determined by bioluminescence (10^6 to 10^8 p/s/cm^2/sr of average radiance). Mice were sacrificed 1 h after administration, and tumors were processed as described above.

To evaluate the BBB disruption, 6–8 weeks athymic nude littermates bearing similar intracranial tumors were injected i.p. with 400 µL of 4% Evan's blue dye (Sigma). One hour after injection, mice were sacrificed by CO_2 inhalation and perfused with acidified fixative (1% PFA in 0.05 mM citrate buffer, pH 3.5). Collected brain tumors and samples of their contralateral hemisphere were incubated in 700 µL of formamide (Sigma) to extract Evan's blue at 60 °C overnight. Absorbance was measured at 610 nm and 740 nm on a Synergy HT multi-mode microplate reader (BioTek). Non-injected or intracranially injected with 2 µL of PBS (mock surgery), 6–8 weeks athymic nude littermates were included as intact brain controls.

To evaluate the bioavailability of nanobodies plasma and urine samples were obtained from mice sacrificed 15 min, 30 min, 1 h, 4 h, and 24 h after administration of nanobodies. Protein content was measured in plasma and urine samples using a Synergy HT multi-mode microplate reader (BioTek) after incubation with Bradford reagent (Bio-Rad Laboratories, Inc). A volume containing 5 µg of protein for plasma and 1 µg for urine was used for immunoblot detection. ReadyTag anti-6-His mAb (1:1,000; clone 6-HIS, BioXCell) and goat anti-mouse IgG IRDye800CW antibody (1:20,000; LI-COR) allowed detection of His-tagged nanobodies in an Odyssey CLx Imaging System (LI-COR). Vehicle-treated healthy mice were used as controls.

Experimental statement. All experiments and methods were performed in accordance with relevant guidelines and regulations.

Data availability

Data supporting the findings of this manuscript are available from the corresponding author upon reasonable request. Data for bioinformatic analysis are deposited in publicly available patient datasets (e.g. RNA-Seq data from The Cancer Genome Atlas (TCGA; https://www.cancer.gov/tcga); gene expression and patient survival data from TCGA Project (TCGA-GBM and TCGA-GBMLGG), the Chinese Glioma Genome Atlas (CGGA, http://www.cgga.org.cn), and the Repository for Molecular Brain Neoplasia Data (REMBRANDT, https://wiki.cancerimagingarchive.net/display/Public/REMBRANDT).

Received: 6 June 2022; Accepted: 27 December 2022
Published online: 30 December 2022

References

1. Louis, D. N. *et al.* The 2021 WHO classification of tumors of the central nervous system: A summary. *Neuro Oncol.* **23**, 1231–1251. https://doi.org/10.1093/NEUONC/NOAB106 (2021).
2. Silantyev, A. S. *et al.* Current and future trends on diagnosis and prognosis of glioblastoma: From molecular biology to proteomics. *Cells* **2019**, 8. https://doi.org/10.3390/cells8080863 (2019).
3. Stupp, R. *et al.* Radiotherapy plus concomitant and adjuvant temozolomide for glioblastoma. *N. Engl. J. Med.* **352**, 987–996. https://doi.org/10.1056/NEJMoa043330 (2005).
4. Stupp, R. *et al.* Effect of tumor-treating fields plus maintenance temozolomide vs maintenance temozolomide alone on survival in patients with glioblastoma a randomized clinical trial. *JAMA-J. Am. Med. Assoc.* **318**, 2306–2316. https://doi.org/10.1001/jama.2017.18718 (2017).
5. Hegi, M. E. *et al.* MGMT gene silencing and benefit from Temozolomide in glioblastoma. *N. Engl. J. Med.* **352**, 997–1003. https://doi.org/10.1056/nejmoa043331 (2005).
6. Molenaar, R. J. *et al.* The combination of IDH1 mutations and MGMT methylation status predicts survival in glioblastoma better than either IDH1 or MGMT alone. *Neuro Oncol.* **16**, 1263–1273. https://doi.org/10.1093/neuonc/nou005 (2014).
7. Pardridge, W. M. The blood-brain barrier: Bottleneck in brain drug development. *Neurotherapeutics* **2**, 3–14. https://doi.org/10.1007/bf03206638 (2005).
8. Pardridge, W. M. Drug transport across the blood–brain barrier. *J. Cereb. Blood Flow Metab.* **32**, 1959–1972. https://doi.org/10.1038/jcbfm.2012.126 (2012).
9. Pepinsky, R. B. *et al.* Exposure levels of anti-LINGO-1 Li81 antibody in the central nervous system and dose-efficacy relationships in rat spinal cord remyelination models after systemic administration. *J. Pharmacol. Exp. Ther.* **339**, 519–529. https://doi.org/10.1124/jpet.111.183483 (2011).
10. Simeon, R. & Chen, Z. In vitro-engineered non-antibody protein therapeutics. *Protein Cell* **9**, 3–14. https://doi.org/10.1007/s13238-017-0386-6 (2018).
11. Muyldermans, S. *et al.* Camelid immunoglobulins and nanobody technology. *Vet. Immunol. Immunopathol.* **128**, 178–183. https://doi.org/10.1016/j.vetimm.2008.10.299 (2008).
12. Ghahroudi, M. A., Desmyter, A., Wyns, L., Hamers, R. & Muyldermans, S. Selection and identification of single domain antibody fragments from camel heavy-chain antibodies. *FEBS Lett.* **414**, 521–526. https://doi.org/10.1016/S0014-5793(97)01062-4 (1997).
13. Abskharon, R. N. N. *et al.* Probing the N-terminal β-sheet conversion in the crystal structure of the human prion protein bound to a nanobody. *J. Am. Chem. Soc.* **136**, 937–944. https://doi.org/10.1021/ja407527p (2014).
14. De Genst, E. *et al.* Molecular basis for the preferential cleft recognition by dromedary heavy-chain antibodies. *Proc. Natl. Acad. Sci. USA* **103**, 4586–4591. https://doi.org/10.1073/pnas.0505379103 (2006).
15. Pothin, E., Lesuisse, D. & Lafaye, P. Brain delivery of single-domain antibodies: A focus on VHH and VNAR. *Pharmaceutics* **12**, 937. https://doi.org/10.3390/pharmaceutics12100937 (2020).
16. Ruiz-López, E. & Schuhmacher, A. J. Transportation of single-domain antibodies through the blood–brain barrier. *Biomolecules* **11**, 1131 (2021).
17. Dean, M., Hamon, Y. & Chimini, G. The human ATP-binding cassette (ABC) transporter superfamily. *J. Lipid Res.* **42**, 1007–1017. https://doi.org/10.1016/S0022-2275(20)31588-1 (2001).
18. Wang, J.-Q. *et al.* Multidrug resistance proteins (MRPs): Structure, function and the overcoming of cancer multidrug resistance. *Drug Resist. Update* **54**, 100743. https://doi.org/10.1016/j.drup.2021.100743 (2021).

19. Kool, M. *et al.* MRP3, an organic anion transporter able to transport anti-cancer drugs. *Proc. Natl. Acad. Sci. USA* **96**, 6914–6919. https://doi.org/10.1073/pnas.96.12.6914 (1999).
20. Bruhn, O. & Cascorbi, I. Polymorphisms of the drug transporters ABCB1, ABCG2, ABCC2 and ABCC3 and their impact on drug bioavailability and clinical relevance. *Expert Opin. Drug Metab. Toxicol.* **10**, 1337–1354. https://doi.org/10.1517/17425255.2014.952630 (2014).
21. Zhao, Y. *et al.* ABCC3 as a marker for multidrug resistance in non-small cell lung cancer. *Sci. Rep.* **3**, 1–6. https://doi.org/10.1038/srep03120 (2013).
22. Adamska, A. *et al.* ABCC3 is a novel target for the treatment of pancreatic cancer. *Adv. Biol. Regul.* **73**, 100634. https://doi.org/10.1016/j.jbior.2019.04.004 (2019).
23. Kuan, C. T. *et al.* MRP3: A molecular target for human glioblastoma multiforme immunotherapy. *BMC Cancer* **2010**, 10. https://doi.org/10.1186/1471-2407-10-468 (2010).
24. Wang, F. *et al.* Identification of a panel of genes as a prognostic biomarker for glioblastoma. *EBioMedicine* **37**, 68–77. https://doi.org/10.1016/j.ebiom.2018.10.024 (2018).
25. Jovčevska, I. *et al.* TRIM28 and β-actin identified via nanobody-based reverse proteomics approach as possible human glioblastoma biomarkers. *PLoS ONE* **9**, 1–22. https://doi.org/10.1371/journal.pone.0113688 (2014).
26. Tomczak, K., Czerwińska, P. & Wiznerowicz, M. The Cancer Genome Atlas (TCGA): An immeasurable source of knowledge. *Współczesna Onkol.* **19**, 68–77. https://doi.org/10.5114/wo.2014.47136 (2015).
27. Ritchie, M. E. *et al.* Limma powers differential expression analyses for RNA-sequencing and microarray studies. *Nucleic Acids Res.* **43**, e47. https://doi.org/10.1093/nar/gkv007 (2015).
28. Bowman, R. L., Wang, Q., Carro, A., Verhaak, R. G. W. & Squatrito, M. GlioVis data portal for visualization and analysis of brain tumor expression datasets. *Neuro Oncol.* **19**, 139–141. https://doi.org/10.1093/neuonc/now247 (2017).
29. Proescholdt, M. A. *et al.* Function of carbonic anhydrase IX in glioblastoma multiforme. *Neuro Oncol.* **14**, 1357–1366. https://doi.org/10.1093/neuonc/nos216 (2012).
30. Araste, F., Ebrahimizadeh, W., Rasooli, I., Rajabibazl, M. & Mousavi Gargari, S. L. A. novel VHH nanobody against the active site (the CA domain) of tumor-associated, carbonic anhydrase isoform IX and its usefulness for cancer diagnosis. *Biotechnol. Lett.* **36**, 21–28. https://doi.org/10.1007/s10529-013-1340-1 (2014).
31. Jespersen, M. C., Peters, B., Nielsen, M. & Marcatili, P. BepiPred-2.0: Improving sequence-based B-cell epitope prediction using conformational epitopes. *Nucleic Acids Res.* **45**, W24–W29. https://doi.org/10.1093/nar/gkx346 (2017).
32. Sanchez-Trincado, J. L., Gomez-Perosanz, M. & Reche, P. A. Fundamentals and methods for T- and B-cell epitope prediction. *J. Immunol. Res.* https://doi.org/10.1155/2017/2680160 (2017).
33. Sun, J. *et al.* Does difference exist between epitope and non-epitope residues? Analysis of the physicochemical and structural properties on conformational epitopes from B-cell protein antigens. *Immunome Res.* **7**, 1–11 (2011).
34. Kringelum, J. V., Nielsen, M., Padkjær, S. B. & Lund, O. Structural analysis of B-cell epitopes in antibody:protein complexes. *Mol. Immunol.* **53**, 24–34. https://doi.org/10.1016/j.molimm.2012.06.001 (2013).
35. Pontén, F., Jirström, K. & Uhlen, M. The human protein Atlas—A tool for pathology. *J. Pathol.* **216**, 387–393. https://doi.org/10.1002/path.2440 (2008).
36. Muyldermans, S. Nanobodies: Natural single-domain antibodies. *Annu. Rev. Biochem.* **82**, 775–797. https://doi.org/10.1146/ANNUREV-BIOCHEM-063011-092449 (2013).
37. Steeland, S., Vandenbroucke, R. E. & Libert, C. Nanobodies as therapeutics: Big opportunities for small antibodies. *Drug Discov. Today* **21**, 1076–1113. https://doi.org/10.1016/j.drudis.2016.04.003 (2016).
38. Jovčevska, I. & Muyldermans, S. The therapeutic potential of nanobodies. *BioDrugs* **34**, 11–26 (2020).
39. Kazerooni, A. F. *et al.* Multi-omic prediction of overall survival in patients with glioblastoma : Additive and synergistic value of clinical measures, radiomics, and genomics. *Sci. Rep.* https://doi.org/10.21203/rs.3.rs-908405/v1License (2021).
40. Chua, C. *et al.* Characterization of a side population of astrocytoma cells in response to temozolomide. *J. Neurosurg.* **109**, 856–866. https://doi.org/10.3171/JNS/2008/109/11/0856 (2008).
41. Liu, Y. *et al.* Effect of siRNA-Livin on drug resistance to chemotherapy in glioma U251 cells and CD133+ stem cells. *Exp. Ther. Med.* **10**, 1317–1323. https://doi.org/10.3892/etm.2015.2675 (2015).
42. Pessina, S. *et al.* The multidrug-resistance transporter Abcc3 protects NK cells from chemotherapy in a murine model of malignant glioma. *Oncoimmunology* **5**, 1–13. https://doi.org/10.1080/2162402X.2015.1108513 (2016).
43. Pellegatta, I., Pessina, P. & Anghileri, E. Finocchiaro ABCC3 expressed by CD56dim CD16+ NK cells predicts response in glioblastoma patients treated with combined chemotherapy and dendritic cell immunotherapy. *Int. J. Mol. Sci.* **20**, 5886. https://doi.org/10.3390/ijms20235886 (2019).
44. Zhang, Q. *et al.* Development of a prognostic five-gene signature for diffuse lower-grade glioma patients. *Front. Neurol.* **12**, 1–10. https://doi.org/10.3389/fneur.2021.633390 (2021).
45. Jeon, H. M. *et al.* ID4 imparts chemoresistance and cancer stemness to glioma cells by derepressing miR-9*-mediated suppression of SOX2. *Cancer Res.* **71**, 3410–3421. https://doi.org/10.1158/0008-5472.CAN-10-3340 (2011).
46. Kuan, C. T. *et al.* Recombinant single-chain variable fragment antibodies against extracellular epitopes of human multidrug resistance protein MRP3 for targeting malignant gliomas. *Int. J. Cancer* **127**, 598–611. https://doi.org/10.1002/ijc.25062 (2010).
47. Škrlj, N. *et al.* Recombinant single-chain antibody with the trojan peptide penetratin positioned in the linker region enables cargo transfer across the blood-brain barrier. *Appl. Biochem. Biotechnol.* **169**, 159–169. https://doi.org/10.1007/s12010-012-9962-7 (2013).
48. Van de Water, J. A. J. M. *et al.* Therapeutic stem cells expressing variants of EGFR-specific nanobodies have antitumor effects. *Proc. Natl. Acad. Sci. USA* **109**, 16642–16647. https://doi.org/10.1073/pnas.1202832109 (2012).
49. Samec, N. *et al.* Glioblastoma-specific anti-TUFM nanobody for in-vitro immunoimaging and cancer stem cell targeting. *Oncotarget* **9**, 17282–17299. https://doi.org/10.18632/oncotarget.24629 (2018).
50. Zottel, A. *et al.* Anti-vimentin, anti-TUFM, anti-NAP1L1 and anti-DPYSL2 nanobodies display cytotoxic effect and reduce glioblastoma cell migration. *Ther. Adv. Med. Oncol.* https://doi.org/10.1177/1758835920915302 (2020).
51. Mir, M. A., Mehraj, U., Sheikh, B. A. & Hamdani, S. S. Nanobodies: The "magic bullets" in therapeutics, drug delivery and diagnostics. *Hum. Antibodies* **28**, 29–51. https://doi.org/10.3233/HAB-190390 (2020).
52. De Groof, T. W. M. *et al.* Nanobody-targeted photodynamic therapy selectively kills viral GPCR-expressing glioblastoma cells. *Mol. Pharm.* https://doi.org/10.1021/acs.molpharmaceut.9b00360 (2019).
53. Huang, H. *et al.* Modular design of nanobody-drug conjugates for targeted-delivery of platinum anticancer drugs with an MRI contrast agent. *Chem. Commun.* **55**, 5175–5178. https://doi.org/10.1039/c9cc01391a (2019).
54. Debie, P., Devoogdt, N. & Hernot, S. Targeted nanobody-based molecular tracers for nuclear imaging and image-guided surgery. *Antibodies* **8**, 12. https://doi.org/10.3390/antib8010012 (2019).
55. Bao, C. *et al.* The application of nanobody in CAR-T therapy. *Biomolecules* **11**, 238. https://doi.org/10.3390/biom11020238 (2021).
56. Marino, M. *et al.* AAV-mediated delivery of an anti-BACE1 VHH alleviates pathology in an Alzheimer's disease model. *EMBO Mol. Med.* **14**, 1–21. https://doi.org/10.15252/emmm.201809824 (2022).
57. Duggan, S. Caplacizumab: First global approval. *Drugs* **78**, 1639–1642. https://doi.org/10.1007/s40265-018-0989-0 (2018).
58. Ruiz-López, E. *et al.* Diagnosis of glioblastoma by immuno-positron emission tomography. *Cancers (Basel).* **14**, 74. https://doi.org/10.3390/cancers14010074 (2021).

59. Vosjan, M. J. W. D. *et al.* Nanobodies targeting the hepatocyte growth factor: Potential new drugs for molecular cancer therapy. *Mol. Cancer Ther.* **11**, 1017–1025. https://doi.org/10.1158/1535-7163.MCT-11-0891 (2012).
60. Binder, J. X. *et al.* COMPARTMENTS: Unification and visualization of protein subcellular localization evidence. *Database* **2014**, bau012. https://doi.org/10.1093/database/bau012 (2014).
61. Zhao, Z. *et al.* Chinese Glioma Genome Atlas (CGGA): A comprehensive resource with functional genomic data from Chinese glioma patients. *Genomics Proteomics Bioinform.* **19**, 1–12. https://doi.org/10.1016/j.gpb.2020.10.005 (2021).
62. Gusev, Y. *et al.* Data descriptor: The REMBRANDT study, a large collection of genomic data from brain cancer patients. *Sci. Data* **5**, 1–9. https://doi.org/10.1038/sdata.2018.158 (2018).
63. Ghassabeh, G.H., Saerens, D., & Muyldermans, S. Isolation of antigen-specific nanobodies. in *Antibody Engineering*. 251–266. ISBN 9783642011474 (2010).
64. Conrath, K. E. *et al.* β-Lactamase inhibitors derived from single-domain antibody fragments elicited in the Camelidae. *Antimicrob. Agents Chemother.* **45**, 2807–2812. https://doi.org/10.1128/AAC.45.10.2807-2812.2001 (2001).
65. Pyonteck, S. M. *et al.* CSF-1R inhibition alters macrophage polarization and blocks glioma progression. *Nat. Med.* **19**, 1264–1272. https://doi.org/10.1038/nm.3337 (2013).
66. De Lucas, A. G. *et al.* Targeting MT1-MMP as an immunoPET-based strategy for imaging gliomas. *PLoS ONE* **11**, 1–19. https://doi.org/10.1371/journal.pone.0158634 (2016).

Acknowledgements

A.J.S., E.R.-L, and I.J thank Prof. Radovan Komel for his support and advice. A.J.S. and E.R.-L would like to thank prof. Radovan Komel for accepting E.R.-L as part of his laboratory as a short-term exchange student under the mentorship of I.J within the Ibercaja-CAI Research Fellowships program (REF.: CM 5/19). A.J.S., E.R.-L. and R.G-G. thank the Molecular Oncology Lab members at IIS Aragón for critical reading of the manuscript. The contribution of A.J.S. honors the memory of "Julito" (Julio César López Navarro), Eduardo Lastrada, Óscar Lou and Dr. José Baselga whose absences inspire our work every day in the laboratory. The contribution of E.R.-L., R.G-G and A.J.S. honor the memory of Dr. Nacho Bon Romero and Celia Pascual Sanz. This research was funded by Instituto de Salud Carlos III through the Fondo de Investigación en Salud Projects "PI18/01665" and "PI21/00441" and co-funded by European Union (ERDF, "A way to make Europe"), the XIII Beca FERO en Investigación Oncológica Traslacional from Fundación FERO, Ayudas a la investigación del cáncer infantil from Asociación de Padres de Niños con Cáncer de Aragón (ASPANOA), Proyectos líneas prioritarias y de carácter multidisciplinar de la RIS3 2021-2023 DGA (LMP248_21), and Metapremio from the Asociación Española de Cáncer de Mama Metastásico (A.J.S.), Ayuda Predoctoral-Aragón from Asociación Española Contra el Cáncer (AECC) and Fundación Científica AECC (REF.: PRDAR17002RUIZ) and Ibercaja-CAI Research Fellowships program (REF.: CM 5/19) (E.R.-L), and by post-doctoral project Z3-1869 from Slovenian research Agency (I.J.).

Author contributions

Conceptualization, A.J.S.; methodology, A.J.S., E.R.-L., I.J., R.G.-G., H.T., S.M.; validation, E.R.-L.; formal analysis, E.R.-L.; investigation, E.R.-L., I.J.; resources, A.J.S.; bioinformatic analysis H.T., F.A.-S., A.J.S.; writing—original draft preparation, A.J.S., E.R.-L. I.J.; writing—review and editing, A.J.S., E.R.-L. I.J., R.G.-G., H.T., F.A.-S, S.M.; supervision, A.J.S.; project administration, A.J.S.; funding acquisition, A.J.S. All authors have read and agreed to the published version of the manuscript.

Competing interests

The authors declare no competing interests.

Additional information

Supplementary Information The online version contains supplementary material available at https://doi.org/10.1038/s41598-022-27161-3.

Correspondence and requests for materials should be addressed to A.J.S.

Reprints and permissions information is available at www.nature.com/reprints.

Publisher's note Springer Nature remains neutral with regard to jurisdictional claims in published maps and institutional affiliations.